Rotational bands in ^{135}Ce: Collective prolate and oblate rotation

R. Ma, E. S. Paul,* D. B. Fossan, Y. Liang, and N. Xu
Department of Physics, State University of New York at Stony Brook, Stony Brook, New York 11794

R. Wadsworth
Department of Physics, University of York, Heslington, York Y01 5DD, United Kingdom

I. Jenkins and P. J. Nolan
Oliver Lodge Laboratory, University of Liverpool, P.O. Box 147, Liverpool L69 3BX, United Kingdom
(Received 11 December 1989)

Several rotational bands have been established in the $N=77$ ^{135}Ce nucleus following the ^{122}Sn(^{18}O,$5n\gamma$) reaction. At low spins, the yrast band, built on an orbital from the top of the $\nu h_{11/2}$ shell, exhibits a large signature splitting of $\sim$300 keV implying a significant deviation from axial symmetry ($\gamma \ll 0°$). At higher spins, three $\Delta I=1$ bands were established. Two of these bands are built on prolate ($\gamma \sim 0°$) mixed neutron-proton configurations as systematically observed in several $N=75$ isotones. The third of these bands shows properties similar to those observed for collectively rotating ($\gamma \sim -60°$) mixed neutron-proton configurations as recently reported in nearby odd-Z, doubly odd, and even-even nuclei. The present study represents the first observation of such a band in an odd-N nucleus. In addition, two decoupled $\Delta I=2$ bands, built on oblate three-quasineutron configurations, were observed.

I. INTRODUCTION

Odd-N nuclei in the light rare-earth region with neutron numbers $N>74$ exhibit low-spin yrast rotational bands built on neutron orbitals from the top of the $h_{11/2}$ shell. Such bands exhibit extraordinarily large signature splittings, that cannot be explained with axially symmetric deformations, implying nuclear shapes with a significant degree of triaxiality. For a prolate shape, high-Ω ($\frac{9}{2}$,$\frac{11}{2}$) components of the $h_{11/2}$ shell are near the Fermi surface which would lead to rotational bands with vanishingly small signature splittings. However, for the collective oblate shape ($\gamma=-60°$, Lund convention[1]), low-Ω ($\frac{1}{2}$,$\frac{3}{2}$) components are near the Fermi surface which would give rise to rotational bands with maximal signature splitting. When compared to cranked shell-model calculations, the experimentally observed signature splittings in the $N=75,77$ nuclei imply intermediate values of γ in the collective regime $-60° \leq \gamma \leq 0°$. Moreover, recent theoretical calculations[2-4] predict shapes with $\gamma \sim -30°$ for the ground-state bands of such nuclei with neutron numbers in excess of 74.

An additional feature of nuclei in this mass region is that they are predicted to show shallow[2,5,6] energy potentials with respect to γ, and as a consequence the nuclear shape can be stabilized at different specific values of γ by the occupation of various high-j quasiparticle orbitals.[7,8] In addition, at higher rotational frequencies, shape changes can readily be achieved by the rotational alignment of specific quasiparticle pairs. For the odd-N nuclei with significant triaxiality at low spin, the rotational alignment of both $\pi h_{11/2}$ and $\nu h_{11/2}$ pairs is predicted to occur at similar rotational frequencies; the proton alignment induces a shape change to prolate ($\gamma \sim 0°$) while the neutron alignment can induce a change to the collectively rotating oblate ($\gamma \sim -60°$) shape.[9] Thus, nuclei in this mass region are ideal for studying shape-coexistence phenomena.

There is increasing evidence for strongly coupled $\Delta I=1$ bands built on oblate ($\gamma \sim -60°$) multiparticle configurations in odd-Z,[10-12] doubly odd,[13] and even-even[14,15] nuclei in this mass region. The systematics of these bands are discussed in Ref. 15. A similar $\Delta I=1$ rotational band has been observed in ^{135}Ce from the current experiment; these results extend, for the first time, the systematics of such bands to an odd-N nucleus.

The present study of ^{135}Ce forms part of a systematic study of odd-N nuclei recently undertaken at Stony Brook. Previously, this work has concentrated on $N=75$ nuclei[9,16-19] ranging from barium ($Z=56$) up to gadolinium ($Z=64$). The heavier $N=77$ isotones, being less deformed and more γ soft, may be expected to show an even richer structure dominated by the shape-driving (γ) effects of the occupied quasiparticle orbitals. Low-lying states in ^{135}Ce have previously been investigated by Droste *et al.*[20] In addition, the low-spin $\nu h_{11/2}$ yrast band was observed up to $I^{\pi}=\frac{19}{2}^{-}$ by Gizon *et al.*,[21] and a $\frac{19}{2}^{+}$ isomer established with an 8-ns half-life; the g factor of this isomeric state has been measured by Zemel *et al.*[22]

II. EXPERIMENTAL METHODS AND RESULTS

A. Coincidence experiments

The ^{122}Sn(^{18}O,$xn\gamma$)$^{140-x}$Ce reaction at beam energies of 85 and 89 MeV was used to investigate high-spin states

 ©1990 The American Physical Society

of the $^{134-136}$Ce nuclei. Results for even-even ^{136}Ce have been published elsewhere.[15] Two stacked self-supporting ^{122}Sn targets of thickness 500 μg/cm^2 were bombarded by beams of ^{18}O ions accelerated at the Stony Brook Superconducting LINAC Facility such that the majority of the recoiling nuclei left the target material with the full recoil velocity prior to γ-ray emission. An array of six bismuth germanate (BGO) Compton-suppressed Ge detectors[23] was used to record γ-γ coincidence data. In order to improve the resolution of the fully Doppler-shifted transitions, lead tapered-slit collimators were inserted in front of the Ge detectors such that an opening half-angle $\Delta(\theta/2)=4.6°$ was achieved. In-beam resolutions of about 3.0 keV for 1-MeV γ rays were typical. In addition, γ-ray multiplicity information was recorded using 14 hexagonal bismuth germanate crystals covering a solid angle in excess of 80% of 4π.

In order to reduce background activity and Coulex lines, only those Ge-Ge events in coincidence with at least two BGO elements were written onto magnetic tape for subsequent off-line analysis. Under this condition, approximately 120 million two- or higher-order Ge-Ge events were recorded at 85 MeV while 160 million events were recorded at 89 MeV. All the events taken at 85 MeV were sorted off line into an E_γ-E_γ array, while for the events recorded at 89 MeV only those events with fold (defined as the number of BGO elements firing) $k \leq 10$ were sorted into this array. This requirement was undertaken to reduce the strong $4n$ channel into ^{136}Ce relative to the $5n$ channel into ^{135}Ce. The higher-order coincidence Ge events (triples, quadrupoles, etc.), less than 2% of total, were decomposed into double events during the off-line analysis. The background, arising from many weak unresolved continuum γ rays and from Compton scattering of the strong discrete lines, was subtracted channel by channel from the γ-γ array using the method outlined in Ref. 24.

Gated spectra generated from the background-subtracted array were used to construct the decay scheme of ^{135}Ce which is presented in Fig. 1, while examples of such coincidence spectra are shown in Fig. 2. These spectra represent the sum of several transitions in bands 1 and 5. Since these bands both decay through a $\frac{19}{2}^+$ isomer of $t_{1/2}=8$ ns (band 2), the transitions below this isomer show both Doppler-shifted and -unshifted components. The main component is the fully shifted component emitted in flight. However, the recoiling nuclei from the first target foil may stop in the second foil, or those from the second in a lead beam-stop placed $\sim$1 cm downsteram of the target foils, prior to emitting the de-

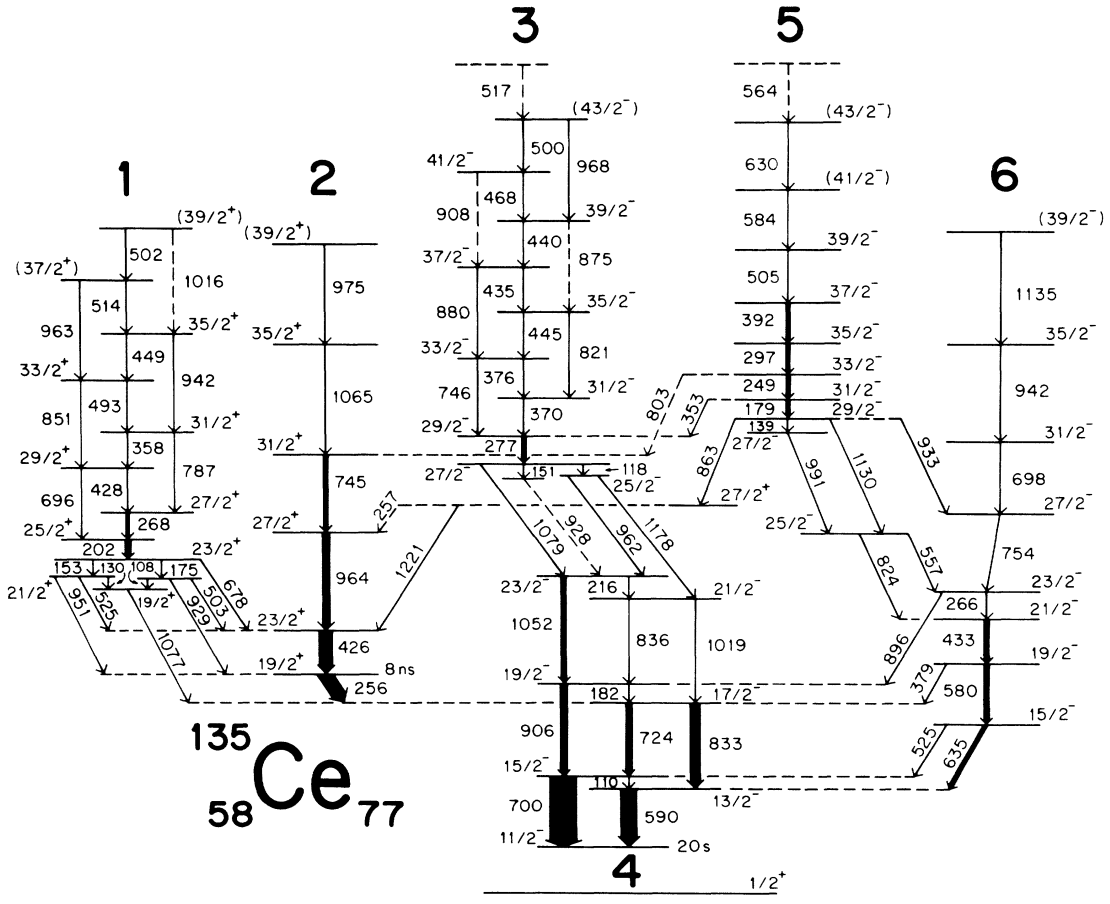

FIG. 1. The decay scheme of ^{135}Ce deduced from this work. The transition energies are given in keV and the widths of the arrows indicate their relative intensities. The decay of the $\frac{11}{2}^-$ isomer which is at an excitation energy of 445 keV to the $\frac{1}{2}^+$ ground state is given in Ref. 20.

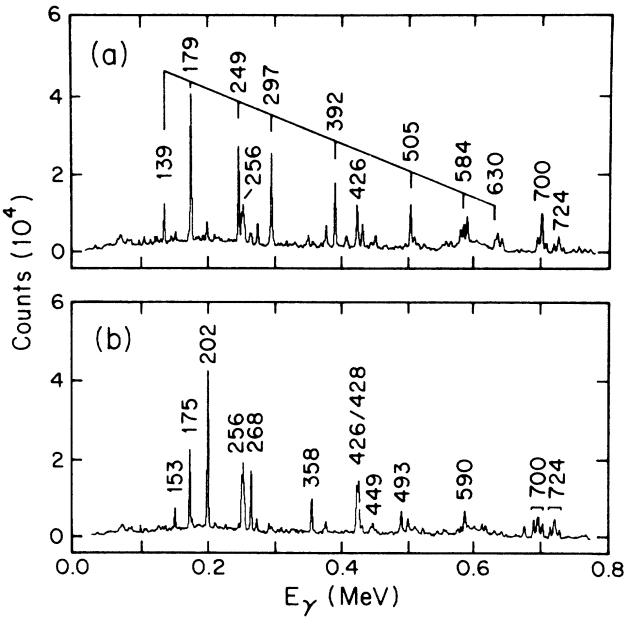

FIG. 2. Representative coincidence spectra obtained from the background-subtracted E_γ-E_γ array. The transition energies are labeled in keV. (a) A sum of gates associated with band 5; gates have been set on the 139-, 249-, 297-, and 392-keV transitions. (b) A sum of gates set on the 268-, 428-, 358-, and 493-keV transitions of band 1. Because of the 8-ns $\frac{19}{2}^+$ isomer, the transitions below the isomer (256, 700, and 724 keV) show stopped components as discussed in the text.

layed transitions below the isomer; all three have the same effective solid angle for detection. Because of the detector geometry with detectors at forward, backward, and 90° angles, three peaks are evident in Fig. 2 for the 700- and 724-keV transitions while the 256-keV transition is broadened.

B. Angular-distribution and correlation data

Both angular-distribution and correlation experiments were performed to seek information on the γ-ray multipolarities. The angular-distribution data, taken in singles, provide the most information for intensities and mixing ratios; however, in cases where the γ rays cannot be resolved in singles spectra, the angular correlation analysis using coincidence data is especially useful. Although these results do not provide rigorous information on the relative parity, mixed transitions strongly imply the same parity for the initial and final states because of the drastic difference in the magnetic and electric transition probabilities of the same multipole order.

The angular-distribution measurement was undertaken for the transitions in ^{135,136}Ce using the ^{124}Sn(^{16}O,$xn\gamma$)$^{140-x}$Ce reaction. A 91-MeV ^{16}O beam was used to bombard a ^{124}Sn target of thickness 2.3 mg/cm^2, rolled onto a natural lead backing of 50 mg/cm^2, producing ^{135}Ce nuclei via the $5n$ channel. One Compton-suppressed Ge detector, 22 cm from the target, was positioned at angles 90°, 115°, 125°, 135°, and 145° with respect to the beam direction. A second Ge detector at −90° served as a monitor. The empirical γ-ray intensities were fitted to the standard Legendre expansion

$$W(\theta)=A_0+A_2P_2(\cos\theta)+A_4P_4(\cos\theta)\ , \qquad (1)$$

where A_0, A_2, and A_4 are adjustable parameters. The results of this analysis are presented in Table I where a small correction has been made to each A_2/A_0 and A_4/A_0 value to account for the finite size of the detector. For other transitions assigned to ^{135}Ce that were weak or formed doublets in the singles spectra, the intensities were obtained from the coincidence data. These

TABLE I. Energies, intensities, and angular-distribution data for the transitions assigned to ^{135}Ce following the ^{122}Sn(^{18}O,$5n\gamma$) reaction at 85 and 89 MeV.

E_γ[a] keV	Rel. I_γ[b]	A_2/A_0	A_4/A_0	DCO[c] ratio	Mult.	Assignment, mixing ratio
108.0	<2			0.3(1)	$M1/E2$	$\frac{21}{2}^+\rightarrow\frac{19}{2}^+$
109.5	<1				$M1/E2$	$\frac{15}{2}^-\rightarrow\frac{13}{2}^-$
117.9	5			0.60(5)	$M1/E2$	$\frac{27}{2}^-\rightarrow\frac{25}{2}^-$
129.8	<2				$M1/E2$	$\frac{21}{2}^+\rightarrow\frac{19}{2}^+$
139.1	<2			0.35(5)	$M1/E2$	$\frac{29}{2}^-\rightarrow\frac{27}{2}^-$
150.7	9			0.77(5)	($M1/E2$)	$\frac{27}{2}^-\rightarrow\frac{25}{2}^-$
152.7	<2			0.5(1)	$M1/E2$	$\frac{23}{2}^+\rightarrow\frac{21}{2}^+$
175.1	10	−0.158(40)	+0.108(55)	0.8(1)	$M1/E2$	$\frac{23}{2}^+\rightarrow\frac{21}{2}^+$ $\delta=0.05\pm0.08$
178.5	11	−0.135(39)	+0.086(53)	0.6(1)	$M1/E2$	$\frac{31}{2}^-\rightarrow\frac{29}{2}^-$ $\delta=0.06\pm0.07$
181.9	<2				$M1/E2$	$\frac{19}{2}^-\rightarrow\frac{17}{2}^-$
202.1[d]	27	−0.129(33)	+0.101(46)	0.43(3)	$M1/E2$	$\frac{25}{2}^+\rightarrow\frac{23}{2}^+$ $\delta=0.07\pm0.07$

TABLE I. (*Continued*).

E_γ[a] keV	Rel. I_γ[b]	A_2/A_0	A_4/A_0	DCO[c] ratio	Mult.	Assignment, mixing ratio
216	<1				$M1/E2$	$\frac{23}{2}^- \rightarrow \frac{21}{2}^-$
249.0	10	−0.255(42)	+0.065(57)	0.31(5)	$M1/E2$	$\frac{33}{2}^- \rightarrow \frac{31}{2}^+$
						$\delta = -0.02^{+0.04}_{-0.06}$
256.0	70	−0.089(32)[e]	+0.077(44)[e]		$E1$	$\frac{19}{2}^+ \rightarrow \frac{17}{2}^-$
257	<2				$M1/E2$	$\frac{27}{2}^+ \rightarrow \frac{27}{2}^+$
265.7	9			0.84(3)	$M1/E2$	$\frac{23}{2}^- \rightarrow \frac{21}{2}^-$
268.0	16	−0.356(35)	+0.031(50)	0.49(3)	$M1/E2$	$\frac{27}{2}^+ \rightarrow \frac{25}{2}^+$
						$\delta = -0.07 \pm 0.02$
277.1	15	−0.280(35)	+0.073(50)	0.36(3)	$M1/E2$	$\frac{29}{2}^- \rightarrow \frac{27}{2}^-$
						$\delta = -0.03 \pm 0.05$
297.5[d]	10			0.59(3)	$M1/E2$	$\frac{35}{2}^- \rightarrow \frac{33}{2}^-$
352.4	2			0.4(1)	$M1/E2$	$\frac{31}{2}^- \rightarrow \frac{29}{2}^-$
358.2	10	−0.332(47)	+0.108(65)	0.87(5)	$M1/E2$	$\frac{31}{2}^+ \rightarrow \frac{29}{2}^+$
						$\delta = -0.06 \pm 0.07$
370.0	6	−0.412(57)	+0.083(78)	0.60(4)	$M1/E2$	$\frac{31}{2}^- \rightarrow \frac{29}{2}^-$
						$\delta = -0.10 \pm 0.06$
375.6	4			0.63(5)	$M1/E2$	$\frac{33}{2}^- \rightarrow \frac{31}{2}^-$
379.2	6			0.58(5)	$M1/E2$	$\frac{19}{2}^- \rightarrow \frac{17}{2}^-$
392.2	10	−0.291(47)	+0.082(65)	0.51(4)	$M1/E2$	$\frac{37}{2}^- \rightarrow \frac{35}{2}^-$
						$\delta = -0.04 \pm 0.06$
425.6	47	+0.443(39)	+0.013(45)		$E2$	$\frac{23}{2}^+ \rightarrow \frac{19}{2}^+$
428.3	11	−0.430(39)	+0.028(55)	0.61(6)	$M1/E2$	$\frac{29}{2}^+ \rightarrow \frac{27}{2}^+$
						$\delta = -0.11 \pm 0.03$
433.5	11	−0.508(42)	+0.066(59)	0.2(1)	$M1/E2$	$\frac{21}{2}^- \rightarrow \frac{19}{2}^-$
						$\delta = -0.16 \pm 0.04$
434.9	11	−0.523(41)	+0.067(59)	0.3(1)	$M1/E2$	$\frac{37}{2}^- \rightarrow \frac{35}{2}^-$
						$\delta = -0.18 \pm 0.05$
440.0	6	−0.548(58)	+0.113(79)	0.27(6)	$M1/E2$	$\frac{39}{2}^- \rightarrow \frac{37}{2}^-$
						$\delta = -0.19^{+0.08}_{-0.11}$
445.1[d]	13	−0.605(40)	+0.027(58)	0.32(4)	$M1/E2$	$\frac{35}{2}^- \rightarrow \frac{33}{2}^-$
						$\delta = -0.23 \pm 0.03$
449.2	5			0.4(1)	$M1/E2$	$\frac{35}{2}^+ \rightarrow \frac{33}{2}^+$
468.0	3			0.5(1)	$M1/E2$	$\frac{41}{2}^- \rightarrow \frac{39}{2}^-$
492.9	7			0.6(1)	$M1/E2$	$\frac{33}{2}^+ \rightarrow \frac{31}{2}^+$
500	<2			0.7(1)	$(M1/E2)$	$(\frac{43}{2}^-) \rightarrow \frac{41}{2}^-$
502	<2				$(M1/E2)$	$(\frac{39}{2}^+ \rightarrow \frac{37}{2}^+)$
503.1	4			1.0(1)	$M1/E2$	$\frac{21}{2}^+ \rightarrow \frac{23}{2}^+$
504.6	6			0.5(1)	$M1/E2$	$\frac{39}{2}^- \rightarrow \frac{37}{2}^-$
514	<2				$(M1/E2)$	$(\frac{37}{2}^+) \rightarrow \frac{35}{2}^+$
517	<2				$(M1/E2)$	$(\frac{45}{2}^-) \rightarrow \frac{43}{2}^-$
525	<2			0.3(1)	$M1/E2$	$\frac{15}{2}^- \rightarrow \frac{15}{2}^-$
525.2	3			0.7(1)	$M1/E2$	$\frac{21}{2}^+ \rightarrow \frac{23}{2}^+$
557.3	3			0.55(5)	$M1/E2$	$\frac{25}{2}^- \rightarrow \frac{23}{2}^-$
564	<2					
579.5	16	+0.305(52)	−0.010(64)	1.5(1)	$E2$	$\frac{19}{2}^- \rightarrow \frac{15}{2}^-$

TABLE I. (*Continued*).

E_γ[a] keV	Rel. I_γ[b]	A_2/A_0	A_4/A_0	DCO[c] ratio	Mult.	Assignment, mixing ratio
583.6	4				$(M1/E2)$	$(\frac{41}{2}^-)\rightarrow\frac{39}{2}^-$
589.7	55	−0.858(29)	+0.093(45)	0.34(3)	$M1/E2$	$\frac{13}{2}^-\rightarrow\frac{11}{2}^-$
						$\delta=-0.42^{+0.06}_{-0.10}$
630	3				$(M1/E2)$	$(\frac{43}{2}^-\rightarrow\frac{41}{2}^-)$
634.9[d]	24	−0.216(35)	+0.070(49)	0.3(1)	$M1/E2$	$\frac{15}{2}^-\rightarrow\frac{13}{2}^-$
						$\delta=-0.02\pm0.05$
678	3			0.9(1)	$M1/E2$	$\frac{23}{2}^+\rightarrow\frac{23}{2}^+$
696	<2				$E2$	$\frac{29}{2}^+\rightarrow\frac{25}{2}^+$
698.3	3			1.3(1)	$E2$	$\frac{31}{2}^-\rightarrow\frac{27}{2}^-$
699.6	≡100	+0.363(37)	−0.008(43)		$E2$	$\frac{15}{2}^-\rightarrow\frac{11}{2}^-$
724.3	19	−0.697(28)	+0.010(45)	0.39(5)	$M1/E2$	$\frac{17}{2}^-\rightarrow\frac{15}{2}^-$
						$\delta=-0.25\pm0.09$
745.0	13	+0.406(47)	−0.024(56)	1.31(4)	$E2$	$\frac{31}{2}^+\rightarrow\frac{27}{2}^+$
746	<2				$E2$	$\frac{33}{2}^-\rightarrow\frac{29}{2}^-$
753.8	8			1.5(1)	$E2$	$\frac{27}{2}^-\rightarrow\frac{23}{2}^-$
786.8	2				$E2$	$\frac{31}{2}^+\rightarrow\frac{27}{2}^+$
803	<2				$E1$	$\frac{33}{2}^-\rightarrow\frac{31}{2}^+$
821	<2			1.1(1)	$E2$	$\frac{35}{2}^-\rightarrow\frac{31}{2}^-$
823.5	3			1.4(1)	$E2$	$\frac{25}{2}^-\rightarrow\frac{21}{2}^-$
833.1	35	+0.372(38)	+0.089(46)		$E2$	$\frac{17}{2}^-\rightarrow\frac{13}{2}^-$
836	5			0.4(1)	$M1/E2$	$\frac{21}{2}^-\rightarrow\frac{19}{2}^-$
851	<2				$E2$	$\frac{33}{2}^+\rightarrow\frac{29}{2}^+$
863.2	5			0.8(1)	$E1$	$\frac{29}{2}^-\rightarrow\frac{27}{2}^+$
875	<2				$E2$	$\frac{39}{2}^-\rightarrow\frac{35}{2}^-$
880	<2			0.9(1)	$E2$	$\frac{37}{2}^-\rightarrow\frac{33}{2}^-$
896	7			0.9(1)	$E2$	$\frac{23}{2}^-\rightarrow\frac{19}{2}^-$
906.2	22	+0.386(42)	−0.067(50)	1.02(3)	$E2$	$\frac{19}{2}^-\rightarrow\frac{15}{2}^-$
908	<2				$E2$	$\frac{41}{2}^-\rightarrow\frac{37}{2}^-$
928	<2				$(M1/E2)$	$(\frac{25}{2}^-)\rightarrow\frac{23}{2}^-$
928.7	4	−0.507(42)	+0.112(59)	0.77(6)	$M1/E2$	$\frac{21}{2}^+\rightarrow\frac{19}{2}^+$
						$\delta=-0.16\pm0.08$
933	<2			0.8(1)	$M1/E2$	$\frac{29}{2}^-\rightarrow\frac{27}{2}^-$
942	2			1.5(1)	$E2$	$\frac{35}{2}^-\rightarrow\frac{31}{2}^-$
942	<2				$E2$	$\frac{35}{2}^+\rightarrow\frac{31}{2}^+$
951.1	<2				$M1/E2$	$\frac{21}{2}^+\rightarrow\frac{19}{2}^+$
962	2			0.4(1)	$M1/E2$	$\frac{25}{2}^-\rightarrow\frac{23}{2}^-$
963	<2				$(E2)$	$(\frac{37}{2}^+)\rightarrow\frac{33}{2}^+$
963.6	26	+0.355(40)	−0.010(48)	1.21(4)	$E2$	$\frac{27}{2}^+\rightarrow\frac{23}{2}^+$
968	<2				$(E2)$	$(\frac{43}{2}^-)\rightarrow\frac{39}{2}^-$
975	<2				$(E2)$	$(\frac{39}{2}^+)\rightarrow\frac{35}{2}^+$
991	<2				$M1/E2$	$\frac{27}{2}^-\rightarrow\frac{25}{2}^-$
1016	<2				$E2$	$\frac{39}{2}^+\rightarrow\frac{35}{2}^+$
1019	5				$E2$	$\frac{21}{2}^-\rightarrow\frac{17}{2}^-$
1052.1	15	+0.232(37)	+0.081(46)	1.3(1)	$E2$	$\frac{23}{2}^-\rightarrow\frac{19}{2}^-$

TABLE I. (*Continued*).

E_γ[a] keV	Rel. I_γ[b]	A_2/A_0	A_4/A_0	DCO[c] ratio	Mult.	Assignment, mixing ratio
1064.9	4	+0.46(10)	+0.06(13)		$E2$	$\frac{35}{2}^+ \rightarrow \frac{31}{2}^+$
1076.6	<2				($E1$)	$\frac{19}{2}^+ \rightarrow \frac{17}{2}^-$
1078.6	4			0.9(1)	$E2$	$\frac{27}{2}^- \rightarrow \frac{23}{2}^-$
1130	3			>1	$E2$	$\frac{29}{2}^- \rightarrow \frac{25}{2}^-$
1135	<2				($E2$)	$(\frac{39}{2}^-) \rightarrow \frac{35}{2}^-$
1178.3	2	+0.46(19)	+0.13(22)		$E2$	$\frac{25}{2}^- \rightarrow \frac{21}{2}^-$
1220.6	5	+0.049(10)	+0.07(13)	1.5(1)	$E2$	$\frac{27}{2}^+ \rightarrow \frac{23}{2}^+$

[a]Transition energies are accurate to ±0.4 keV except those values quoted as integers which are accurate to ±1 keV.
[b]The transition intensities were obtained from a combination of the angular-distribution data and coincidence data. Estimated errors are typically less than 10%.
[c]Angular correlation ratios were obtained from several gating quadrupole transitions.
[d]Doublet with a transition in a neighboring nucleus.
[e]This transition directly depopulates an 8-ns isomer (Ref. 21).

values are also included in Table I. The transition intensities have been corrected for both detector efficiency and internal conversion effects.

The empirical A_2/A_0 and A_4/A_0 angular-distribution coefficients obtained for the $\Delta I=1$ transitions were used to estimate the $E2/M1$ mixing ratios δ for several of these transitions. An average value for the alignment parameter $\alpha_2=0.86(7)$ was obtained from the angular-distribution coefficients for several of the quadrupole transitions. This value was, in turn, used to estimate a value of $\alpha_4=0.65(7)$ using Ref. 25. These alignment parameters and the experimental angular-distribution coefficients were combined with the theoretical angular-distribution functions from Refs. 25 and 26 to extract the $E2/M1$ mixing ratio δ; a χ^2 minimization technique was employed. The results of this analysis are included in Table I where the sign convention of Ref. 25 has been adopted. For good statistical fits of χ^2 vs $\tan^{-1}\delta$, the errors quoted on the mixing ratios reflect uncertainties in the measured experimental quantities; for poorer fits, the errors were derived from a goodness-of-fit criterion.[27]

Since reliable angular distribution coefficients could not be extracted for many of the weaker transitions assigned to ^{135}Ce, an angular correlation analysis was performed making use of the coincidence data. When recording the coincidence data, the six Ge detectors, 14.2 cm distant from the target, had been placed at angles of ±145°, ±28°, −85°, and +80° with respect to the beam axis. The two detectors nearest 90° (−85° and +80°) were sorted against the other four detectors to produce a two-dimensional angular correlation array which had on one axis the two detectors close to 90°, and on the second axis the other four detectors. Empirical directional correlation[28] (DCO) intensity ratios were obtained from this array. Gates were set on known stretched quadrupole transitions along both axes. The intensity ratios of other coincident transitions observed in the two spectra obtained for each gating transition were used to distinguish between stretched dipole and stretched quadrupole transitions. The results of the angular correlation analysis, averaged for several gating stretched quadrupole transitions, are included in Table I.

C. The decay scheme of ^{135}Ce

The decay scheme of ^{135}Ce, deduced from the present study, is shown in Fig. 1. The placement of the γ transitions in the level scheme is based on their coincidence relations and relative intensities. The spin-parity assignments were deduced from the angular-distribution and correlation analysis, together with the observed decay patterns. Six band structures are labeled in the figure in order to facilitate the discussion.

Band 4 is built on a 20-s half-life[20] isomeric state with $I^\pi=\frac{11}{2}^-$ at an excitation energy of 445 keV relative to the $\frac{1}{2}^+$ ground state, and is associated with a high-j unique-parity $\nu h_{11/2}$ orbital. The 700-906-1052- and 833-1019-keV sequences form the two signature components of the low-spin yrast band and are connected by relatively strong high-energy $\Delta I=1$ transitions (590, 724, and 836 keV). In contrast, the low-energy linking $\Delta I=1$ transitions (110, 182, and 216 keV) were found to be of much weaker intensity with only upper limits for their intensities shown in Table I. Large negative A_2/A_0 angular-distribution coefficients extracted for the high-energy 590- and 724-keV $\Delta I=1$ transitions yield negative $E2/M1$ mixing ratios δ for these transitions.

Band 2 is built on an 8-ns half-life[21] $\frac{19}{2}^+$ isomeric state at an excitation energy of 2126 keV. The measured g factor[22] of this state indicates a predominant $\nu s_{1/2}\otimes[\nu h_{11/2}]^2$ three-quasineutron configuration for this level. A series of five quadrupole transitions have been

placed on top of this isomer extending to $I^{\pi}=(\frac{39}{2}^{+})$.

Band 6 consists of an irregular set of negative-parity levels at low spin before developing into a regular band structure at high spin. The lowest state at 1671 keV has been assigned $I^{\pi}=\frac{15}{2}^{-}$; although the angular-distribution data are contaminated by a strong quadrupole transition in neighboring ^{136}Ce, the angular correlation data for the linking 635-keV transition are consistent with the mixed $M1/E2$ $\Delta I=1$ assignment. A quadrupole (580 keV) and two dipole (433 and 266 keV) transitions have been placed above this level extending to $I^{\pi}=\frac{23}{2}^{-}$. The angular-distribution results for the 433-keV transition imply mixed ($\delta<0$) $M1/E2$ $\Delta I=1$ character. The angular distribution for the 266-keV transition could not be extracted due to a contaminant. The angular correlation analysis, however, implies a dipole character for this transition. Furthermore, the decay of a $\frac{25}{2}^{-}$ state via an 824-keV quadrupole and 557-keV dipole imply $\Delta I=1$ for the 266-keV transition. The level depopulated by the 266-keV transition could then possess either $I^{\pi}=\frac{23}{2}^{-}$ or $\frac{23}{2}^{+}$. However, the observation of the 896-keV $\Delta I=2$ transition, feeding the yrast $\frac{19}{2}^{-}$ state, establishes negative parity for this level. The sum of the energies of the 433- and 266-keV transitions is 699 keV; an $E2$ crossover transition of this energy is thus possible between the $\frac{23}{2}^{-}$ and $\frac{19}{2}^{-}$ states. However, the existence of this transition could not be unambiguously determined from the present analysis because of the presence of the 698-700-keV doublet. Four quadrupole transitions (754, 698, 942, and 1135 keV) have been placed on top of the $\frac{23}{2}^{-}$ level extending the band to $I^{\pi}=(\frac{39}{2}^{-})$. A similar negative-parity band structure has recently been established[9] in the lighter $N=75$ ^{131}Ba nucleus.

Bands similar to bands 1 and 3 have systematically been observed[9,16–18] in several $N=75$ isotones. These bands show both signature components and decay predominantly by in-band $M1/E2$ $\Delta I=1$ transitions. Band 1 shows a complicated decay path into the lower-lying states. The spin-parity assignments rely on the empirical angular-distribution and correlation data for the 929- and 175-keV transitions which imply mixed $M1/E2$ $\Delta I=1$ character. Similarly, the angular-distribution data for the in-band $\Delta I=1$ transitions establish the relative spins and parities within the band. Apart from the 202-keV transition, which is contaminated by a transition of similar energy in neighboring ^{136}Ce, the measured angular-distribution coefficients yield negative $E2/M1$ mixing ratios δ for the in-band $\Delta I=1$ transitions, as shown in Table I. Band 3, which decays only into band 4, is assumed to possess negative parity. Again, the in-band $\Delta I=1$ transitions are found to possess negative $E2/M1$ mixing ratios. The $E2$ crossover transitions were observed only weakly and two are shown dashed in Fig. 1.

Band 5 decays by in-band $\Delta I=1$ transitions with none of the $E2$ crossovers being observed. The negative parity for this band is inferred from the observed decay paths and the angular correlation data obtained for several of the depopulating transitions. A bandhead spin-parity assignment of $I^{\pi}=\frac{27}{2}^{-}$ is favored, although an alternative $25/2^{+}$ assignment cannot be conclusively ruled out. The present assignment is supported by the observed DCO ratios for the 353- and 863-keV depopulating transitions which favor mixed ($M1/E2$) and pure ($E1$) dipole assignments, respectively. It has been found empirically, using the defined detector geometry, that the ratios obtained for pure stretched $\Delta I=1$ transitions generally lie in the range 0.6–0.8, while the values obtained for mixed $M1/E2$ $\Delta I=1$ transitions ($\delta<0$) are typically <0.5. These observations are, to some extent, corroborated by the present data when comparing the angular correlation and distribution results. Furthermore, recently published data[9,14] for ^{131,132}Ba greatly support these findings. The present spin-parity assignments for band 5 are also based on the assumption that the depopulating transitions are predominantly of stretched character, i.e., $\Delta I=1,2$ and not $\Delta I=0$ transitions.

III. DISCUSSION

In order to discuss the rotational properties of the six bands shown in Fig. 1, experimental alignments are plotted in Fig. 3 as a function of rotational frequency. The alignment[29] is defined as

$$i_x(\omega)=I_x(\omega)-I_{x,\mathrm{ref}}(\omega)\ , \tag{2}$$

where I_x is estimated as $I_x=[(I+\frac{1}{2})^2-\langle K\rangle^2]^{1/2}$ and $I_{x,\mathrm{ref}}$ is based on a frequency-dependent moment of inertia reference: $\mathcal{J}_{\mathrm{ref}}=\mathcal{J}_0+\omega^2\mathcal{J}_1$. The Harris parameters[30] for the reference were chosen such that the alignment of band 4 is approximately constant; values of $\mathcal{J}_0=3.5\hbar^2$ MeV^{-1} and $\mathcal{J}_1=34.7\hbar^4$ MeV^{-3} were extracted. The choice of $\langle K\rangle$ for each band is discussed in the following sections. Table II summarizes the proposed quasiparticle structures associated with each band.

A. Band 4: The triaxial $\nu h_{11/2}$ band

The low-spin yrast spectroscopy of odd-N nuclei of mass $A\sim135$ is dominated by unique-parity high-j orbitals from the $h_{11/2}$ shell. Indeed the low-spin yrast bands

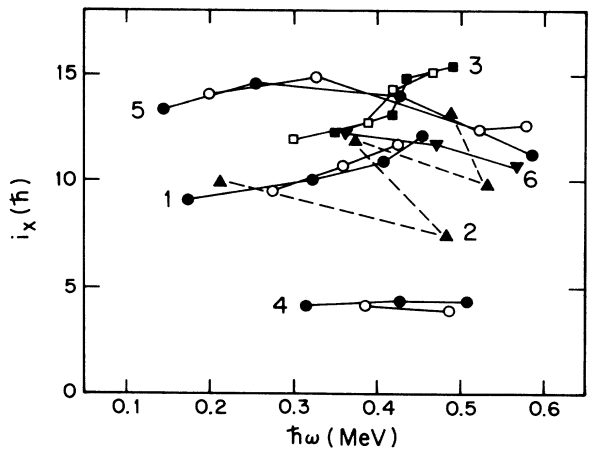

FIG. 3. Experimental alignments for bands 1–6 shown as a function of rotational frequency.

TABLE II. Quasiparticle assignments for the six band structures observed in ^{135}Ce, as shown in Fig. 1. An estimate of the γ deformation for each structure is given.

Band no.	Quasiparticle configuration	Triaxiality γ
1	$\nu h_{11/2}\otimes\pi h_{11/2}\otimes\pi g_{7/2}$	$\sim 0°$
2	$\nu s_{1/2}\otimes[\nu h_{11/2}]^2$	$\sim -60°$
3	$\nu h_{11/2}\otimes[\pi h_{11/2}]^2$	$\sim 0°$
4	$\nu h_{11/2}$	$\sim -30°$
5	$\nu s_{1/2}\otimes[\nu h_{11/2}]^2\otimes\pi h_{11/2}\otimes\pi g_{7/2}$	$\sim -60°$
6	$\nu h_{11/2}\otimes[\nu h_{11/2}]^2$	$\sim -60°$

are associated with such orbitals. For the neutron number $N=77$, the neutron Fermi surface lies near the top of the $h_{11/2}$ shell. In the case of a prolate-deformed nucleus ($\gamma=0°$), the $[505]\frac{11}{2}^-$ Nilsson orbital lies closest to the Fermi surface which would give rise to a strongly coupled rotational band with essentially no signature splitting. In stark contrast, the experimentally extracted signature splitting for band 4 is of the order of 300 keV. Such a large value implies a significant deviation from axial symmetry ($\gamma \ll 0°$) when compared to cranked shell-model calculations. For an axial oblate shape, the $[550]\frac{1}{2}^-$ orbital is close to the Fermi surface which would exhibit maximal signature splitting. However, the ground states of the $N=74$ and 76 core nuclei are predicted[2,3] to possess extremely shallow potential-energy surfaces with respect to the shape-asymmetry parameter γ, but centered around $\gamma\sim -30°$. Assuming a similar triaxial shape for the ^{135}Ce nucleus, low-Ω components of the $h_{11/2}$ shell would be mixed into the wave function for the low-spin yrast band, producing an effective $\langle K\rangle$ intermediate between the extreme values of $\frac{11}{2}$ and $\frac{1}{2}$, and leading to the observation of an appreciable signature splitting. Signature splittings of a similar magnitude have been observed in the $\nu h_{11/2}$ yrast bands of other $N=77$ nuclei[21,31,32] ranging from barium to samarium, and are found to be more than twice as large as those observed in the lighter $N=75$ isotones.[9]

The alignment extracted for band 4 is included in Fig. 3. Since this $\nu h_{11/2}$ configuration is predicted to possess a triaxial shape $\gamma\sim -30°$ midway between prolate ($\gamma=0°,\Omega=\frac{11}{2}$) and oblate ($\gamma=-60°,\Omega=\frac{1}{2}$), an average value of $\langle K\rangle=3$ was used when extracting the alignment.

B. Bands 1 and 3: Proton-aligned bands

Bands similar to bands 1 and 3 have systematically been observed in several $N=75$ isotones.[9,16–18] Characteristics of these bands are the following: (1) in-band decay by predominantly $M1$ $\Delta I=1$ transitions, (2) negative $E2/M1$ mixing ratios for these transitions, and (3) a relatively small signature splitting between the two $\Delta I=2$ components.

By comparison with the $N=75$ isotones, bands 1 and 3 are associated with the positive-parity $\nu h_{11/2}\otimes\pi h_{11/2}\otimes\pi g_{7/2}$ and negative-parity $\nu h_{11/2}\otimes[\pi h_{11/2}]^2$ configurations, respectively. The γ-driving force of the aligned $h_{11/2}$ protons from the bottom of the shell is towards positive values $\gamma>0°$, in contrast to the driving force of the $h_{11/2}$ neutron towards large negative values of γ. For these two three-quasiparticle configurations, the $h_{11/2}$ proton dominates implying near-prolate ($\gamma\sim 0°$), or even $\gamma>0°$, shapes which are reflected experimentally by a relatively small signature splitting.

The alignments of these bands are included in Fig. 3. In the case of band 3, the high-Ω neutron ($\Omega=\frac{11}{2}$ for $\gamma=0°$) is coupled to a pair of rotationally aligned $h_{11/2}$ protons. Therefore, $\langle K\rangle=\frac{11}{2}$ was used in extracting the alignment. For band 1, only the single $h_{11/2}$ proton is rotationally aligned, while the $h_{11/2}$ neutron ($\Omega=\frac{11}{2}$) and $g_{7/2}$ proton ($\Omega=\frac{5}{2}$) are strongly coupled; therefore, $\langle K\rangle=\frac{17}{2}$ was used. When compared to the alignment obtained for the triaxial band 4, the extracted alignments for both bands 1 and 3 using the same procedure are seen to gradually increase with rotational frequency, implying a larger moment of inertia than the reference configuration (band 4). Such an increase may reflect a larger quadrupole deformation for these configurations induced by the occupation of rotationally aligned proton orbitals from the bottom of the $h_{11/2}$ shell. Such orbitals possess the largest polarization effect, related to the $dE/d\beta$ slopes, and would favor larger deformations.

Band 3 shows an anomaly at $\hbar\omega\sim 0.40$ MeV when a gain of alignment $\Delta i_x\sim 2\hbar$ is observed. This increase is much too small to be explained by the rotational alignment of a pair of quasiparticles. However, a simple explanation for this effect would be a change in the $\langle K\rangle$ value for this $\nu h_{11/2}\otimes[\pi h_{11/2}]^2$ configuration induced by a shape change towards negative γ. Indeed, the collective rotation of a γ-soft nucleus could result in a shape change from $\gamma\sim 0°$ towards $\gamma=-30°$ where the collective moment of inertia for irrotational flow is largest. This effect would be reinforced by the shape-driving force of the $h_{11/2}$ neutron to negative γ. Such a shape change would reduce the effective $\langle K\rangle$ value, thus increasing the alignment.

C. Bands 2 and 6: Neutron-aligned bands

Decoupled $\Delta I=2$ rotational bands similar to bands 2 and 6 have recently been established in ^{131}Ba.[9] The measured g factor[22] of the bandhead of band 2 is consistent with a $\nu s_{1/2}\otimes[\nu h_{11/2}]^2$ three-quasineutron configuration. Similar $\frac{19}{2}^+$ three-quasineutron isomers have been observed[21,31] in other $N=77$ nuclei and are related to 5^- $\nu s_{1/2}\otimes\nu h_{11/2}$ states in neighboring even-even nuclei. Because of the strong γ-driving forces of the aligned $h_{11/2}$ neutron pair, the $\nu s_{1/2}\otimes[\nu h_{11/2}]^2$ configuration is expected to possess a shape close to the collectively rotating oblate ($\gamma=-60°$) shape. Similarly, the higher members of band 6 (698-942-1135 keV) may be associated with the oblate $[\nu h_{11/2}]^3$ configuration. Only one signature component of these configurations is strongly populated be-

cause of the large signature splitting of the $\nu h_{11/2}$ and $\nu s_{1/2}$ orbitals for $\gamma \sim -60°$. Recent total-routhian-surface (TRS) cranking calculations have predicted[3,9,33] such oblate nuclear shapes associated with aligned $[h_{11/2}]^2$ neutron states in barium and cerium nuclei.

The alignments extracted for these bands are included in Fig. 3 where $\langle K \rangle = \frac{1}{2}$ has been used because of the rotationally aligned nature of these configurations. The alignment for band 6 is seen to decrease with increasing frequency relative to that of band 4. This effect may be due to a smaller moment of inertia caused by the different collective shapes, i.e., oblate versus triaxial. The alignment for band 2 is extremely irregular and is not characteristic of a rotational band. However, a similar behavior is observed in a related oblate $\nu s_{1/2} \otimes \nu h_{11/2}$ sideband in neighboring ^{136}Ce.[15] As for band 2, this sideband also shows a repeated small-big pattern of $E2$ transitions leading to an irregular zigzag alignment plot.

D. Band 5: A multiquasiparticle oblate band

Perhaps the most interesting finding of the present study is band 5. This band, which was observed with a strong intensity, consists of a regular series of $\Delta I = 1$ transitions, with no signature splitting, extending to high spin and excitation energy. None of the $E2$ crossovers were observed in this band. The alignment, shown in Fig. 3, extracted with $\langle K \rangle = \frac{11}{2}$, is larger than any of the other bands previously discussed. No obvious configuration choice can be made for band 5, however, several speculative structures are discussed below finally leading to a proposed multiquasiparticle configuration with properties consistent with the experiment.

One possibility, is that band 5 is built on a three-quasiparticle structure with negative parity. In order to produce a rotational band with no signature splitting, the odd neutron must occupy the $\nu h_{11/2}[505]\frac{11}{2}^-$ Nilsson orbital at a prolate shape. Furthermore, in order to stabilize the prolate shape, a pair of rotationally aligned low-Ω quasiparticles must be present. The $\nu h_{11/2} \otimes [\pi h_{11/2}]^2$ configuration is already associated with band 3; similar structures have been experimentally established[9,16–19] in several $N=75$ isotones. For rotationally aligned neutrons, the $\nu h_{11/2} \otimes [\nu h_{9/2}]^2$ and $\nu h_{11/2} \otimes [\nu i_{13/2}]^2$ configurations are possibilities. A strong interaction between spin-orbit partners may favor the former, whereas the large alignment would favor the latter. However, neither of these two configurations are expected to significantly enhance the $\Delta I = 1$ $M1$ transitions such that they would dominate the in-band decay. Furthermore, the $\nu h_{9/2}$ and $\nu i_{13/2}$ orbitals lie high above the Fermi surface.

A further problem encountered when consulting the alignment plot of Fig. 3 is that no low-frequency $[\pi h_{11/2}]^2$ band crossing is observed. The blocking of this band crossing implies the presence of at least one $h_{11/2}$ proton. If band 5 were oblate ($\gamma \sim -60°$), configurations containing the strongly coupled $h_{11/2}[505]\frac{11}{2}^-$ *proton* orbital could explain the lack of signature splitting *and* the enhancement of the $M1$ transitions relative to the $E2$ crossovers. The falling of the alignment with rotational frequency, similar to band 6, may indeed point to an oblate shape. The simplest configuration to explain the band properties would then be the positive-parity $\nu h_{11/2} \otimes \pi h_{11/2} \otimes \pi g_{7/2}$ configuration, i.e., the same as for band 1. Bands 1 and 5 would then be built on the same three-quasiparticle configuration but with prolate and oblate shapes, respectively. Although positive parity is not excluded experimentally, the observed alignment of band 5 seems too high for this proposed three-quasiparticle structure.

Furthermore, it is not obvious that a single $h_{11/2}$ neutron could induce such a shape change to $\gamma \sim -60°$. This fact, taken with the large alignment, may imply the presence of several rotationally aligned $h_{11/2}$ neutrons at $\gamma \sim -60°$. The oblate five-quasiparticle $[\nu h_{11/2}]^3 \otimes \pi h_{11/2} \otimes \pi g_{7/2}$ and $\nu s_{1/2} \otimes [\nu h_{11/2}]^2 \otimes \pi h_{11/2} \otimes \pi g_{7/2}$ configurations would indeed show the properties of band 5, i.e., high alignment, no signature splitting, no low-frequency proton band crossing, and strong $M1$ transitions linking the two signatures. The alignment expected for the former five-quasiparticle configuration may be too high and thus the latter configuration is favored. In addition, several other factors favor this choice: first, the $\nu s_{1/2} \otimes [\nu h_{11/2}]^2$ configuration (band 2) lies at a lower excitation energy than the $[\nu h_{11/2}]^3$ configuration (upper part of band 6); second, band 5 decays predominantly, via 863- and 1221-keV transitions, into band 2 associated with the $\nu s_{1/2} \otimes [\nu h_{11/2}]^2$ configuration; and third, the proposed $\nu s_{1/2} \otimes [\nu h_{11/2}]^2 \otimes \pi h_{11/2} \otimes \pi g_{7/2}$ configuration has negative parity as favored experimentally.

In summary, the most plausible configuration for band 5, consistent with the observed band properties, appears to be the collectively rotating oblate ($\gamma \sim -60°$) $\nu s_{1/2} \otimes [\nu h_{11/2}]^2 \otimes \pi h_{11/2} \otimes \pi g_{7/2}$ five-quasiparticle configuration. A remarkably similar band structure, associated with a related oblate configuration involving the last four quasiparticles has recently been established in neighboring ^{136}Ce (Ref. 15) from the present data. In addition, oblate bands associated with the $[\nu h_{11/2}]^2 \otimes \pi h_{11/2}$ configuration have been observed in several odd-Z nuclei of this mass region.[10–12] All of these oblate bands appear as strongly coupled $\Delta I = 1$ bands. The $[\nu h_{11/2}]^2 \otimes \pi h_{11/2}$ part of the configuration has revealed systematic stability for collective oblate bands in this region. The intensity of band 5 may be related to the stability of this oblate band up through several band crossings where feeding into the band can occur to achieve its large population and resulting intensity.

E. Electromagnetic properties

Estimated ratios of reduced transition probabilities, $B(M1; I \rightarrow I-1)/B(E2; I \rightarrow I-2)$ values, are shown in Table III for several of the bands in ^{135}Ce. For most of the ratios, only upper or lower limits could be extracted.

However, values obtained for the $\nu h_{11/2}$ band 4 are seen to be lower than the values obtained for bands 1, 3, and 5. In the case of band 5, the limits were obtained assuming that the unobserved crossover transitions are of less than 1% intensity of the strongest transition, namely the 700-keV $\frac{15}{2}^- \rightarrow \frac{11}{2}^-$ transition of band 4. Similar differences in the $B(M1)/B(E2)$ ratios have been observed[16–18] in the corresponding $\nu h_{11/2}$ (band 4), $\nu h_{11/2} \otimes [\pi h_{11/2}]^2$ (band 3), and $\nu h_{11/2} \otimes \pi h_{11/2} \otimes \pi g_{7/2}$ (band 1) bands in several $N=75$ isotones.

In the geometrical model[34] of Dönau and Frauendorf, the $B(M1)$ rate for $\Delta I=1$ transitions connecting the two signatures of a given configuration can be enhanced by the occupation of strongly coupled quasiparticle orbitals. The magnetic moments of such orbitals lie at large angles with respect to the total spin axis of the nucleus. Hence, the resultant magnetic moments for multiquasiparticle configurations can also lie at appreciable angles to the spin **I**, and the $B(M1)$ rate, proportional to the square of the component of the magnetic moment perpendicular to **I**, is thus increased. The magnitude of the enhancement depends on the K values for various configurations and on the specific quasiparticle g factors; mixed configurations of neutrons and protons usually have strong $M1$ enhancements because the g factors are of opposite sign which results in different **I** and μ directions. For example, the $h_{11/2}$ neutron is associated with the strongly coupled $[505]\frac{11}{2}^-$ orbital for prolate shapes leading to the strong $M1$ transitions in bands 1 and 3. The enhancement for the oblate band 5 occurs because an $h_{11/2}$ *proton* occupies the strongly coupled $[505]\frac{11}{2}^-$ orbital. Since the $h_{11/2}$ proton g factor is much larger than the $h_{11/2}$ neutron g factor ($+1.2$ vs -0.2), the $M1$ transitions should be considerably more enhanced for band 5 as opposed to bands 1 and 3. Indeed, none of the crossover $E2$ transitions were observed in band 5.

TABLE III. Extracted values and limits for $B(M1;I\rightarrow I-1)/B(E2;I\rightarrow I-2)$ ratios for several of the bands in ^{135}Ce.

Spin I ($\hbar$)	$B(M1)/B(E2)$ $(\mu_N/e\,\mathrm{b})^2$
Band 1	
$\frac{29}{2}$	>8
$\frac{31}{2}$	23 ± 7
$\frac{33}{2}$	>9
$\frac{35}{2}$	>14
Band 3	
$\frac{33}{2}$	>6
$\frac{35}{2}$	>19
$\frac{37}{2}$	>24
$\frac{39}{2}$	>13
$\frac{41}{2}$	>6
Band 4	
$\frac{15}{2}$	<1.7
$\frac{17}{2}$	0.40 ± 0.06
$\frac{19}{2}$	<3.2
$\frac{21}{2}$	1.3 ± 0.4
$\frac{23}{2}$	<6
Band 5	
$\frac{31}{2}$	>4
$\frac{33}{2}$	>6
$\frac{35}{2}$	>13
$\frac{37}{2}$	>18
$\frac{39}{2}$	>19
$\frac{41}{2}$	>21
$\frac{43}{2}$	>22

The Dönau and Frauendorf method can also be used to evaluate the $E2/M1$ mixing ratios for multiquasiparticle configurations. Indeed, for the prolate bands 1 and 3, associated with the $\nu h_{11/2} \otimes \pi h_{11/2} \otimes \pi g_{7/2}$ and $\nu h_{11/2} \otimes [\pi h_{11/2}]^2$ configurations, respectively, negative mixing ratios are expected for the $\Delta I=1$ transitions in agreement with experiment. The above method is not applicable for the triaxial shape of band 4; however, a prolatelike $\nu h_{11/2}$ configuration would yield negative mixing ratios. The systematic electromagnetic properties for asymmetric rotors is currently being investigated. Finally, in the case of band 5, if it is assumed that the strongly coupled $h_{11/2}$ proton dominates the configuration, then the negative quadrupole moment associated with the oblate shape is required to reproduce the experimental negative mixing ratios.

IV. CONCLUSIONS

Several band structures have been identified in ^{135}Ce following (HI,xn) reactions. Rotational alignments of both proton pairs, from the bottom of the $h_{11/2}$ shell, and neutron pairs, from the top of the $h_{11/2}$ shell, have been observed. Because of the γ softness of the triaxial core, the proton alignments are associated with prolate ($\gamma\sim0°$) bands while the neutron alignments are associated with collectively rotating oblate ($\gamma\sim-60°$) bands.

A strongly coupled $\Delta I=1$ band has also been established to high spin which is believed to be built on a multiquasiparticle configuration at $\gamma\sim-60°$ containing the $[505]\frac{11}{2}^-$ proton orbital. Bands of similar properties, associated with collective oblate rotation, have recently been established in odd-Z,[10] odd-odd,[13] and even-even[14,15] nuclei, but all with $Z=56$–58. The present band represents the first observation of such a band in an odd-N nucleus ($Z=58$).

ACKNOWLEDGMENTS

This work was supported in part by grants from the National Science Foundation and from the U.K. Science and Engineering Research Council. One of us (I.J.) acknowledges receipt of a United Kingdom Science and Engineering Research Council (SERC) postgraduate studentship during the course of this work.

---

*Present address: Oliver Lodge Laboratory, University of Liverpool, P.O. Box 147, Liverpool L69 3BX, United Kingdom.

[1]G. Andersson, S. E. Larsson, G. Leander, P. Möller, S. G. Nilsson, I. Ragnarsson, S. Åberg, R. Bengtsson, J. Dudek, B. Nerlo-Pomorska, K. Pomorski, and Z. Szymański, Nucl. Phys. **A268**, 205 (1976).

[2]B. D. Kern, R. L. Mlekodaj, G. A. Leander, M. O. Kortelahti, E. F. Zganjar, R. A. Braga, R. W. Fink, C. P. Perez, W. Nazarewicz, and P. B. Semmes, Phys. Rev. C **36**, 1514 (1987).

[3]R. Wyss, private communication.

[4]R. Wyss, J. Nyberg, A. Johnson, R. Bengtsson, and W. Nazarewicz, Phys. Lett. B **215**, 211 (1988).

[5]I. Ragnarrson, A. Sobiczewski, R. K. Sheline, S. E. Larsson, and B. Nerlo-Pomorska, Nucl. Phys. **A233**, 329 (1974).

[6]Y. S. Chen, S. Frauendorf, and G. A. Leander, Phys. Rev. C **28**, 2437 (1983).

[7]G. A. Leander, S. Frauendorf, and F. R. May, in *Proceedings of the Conference on High Angular Momentum Properties of Nuclei, Oak Ridge, 1982,* edited by N. R. Johnson (Harwood Academic, New York, 1983), p. 281.

[8]S. Frauendorf and F. R. May, Phys. Lett. **125B**, 245 (1983).

[9]R. Ma, Y. Liang, E. S. Paul, N. Xu, D. B. Fossan, L. Hildingsson, and R. A. Wyss, Phys. Rev. C **41**, 717 (1990).

[10]E. S. Paul, C. W. Beausang, D. B. Fossan, R. Ma, W. F. Piel, Jr., N. Xu, L. Hildingsson, and G. A. Leander, Phys. Rev. Lett. **58**, 984 (1987).

[11]L. Hildingsson, C. W. Beausang, D. B. Fossan, and W. F. Piel, Jr., Phys. Rev. C **37**, 985 (1988).

[12]N. Xu, C. W. Beausang, R. Ma, E. S. Paul, W. F. Piel, Jr., D. B. Fossan, and L. Hildingsson, Phys. Rev. C **39**, 1799 (1989).

[13]M. J. Godfrey, Y. He, I. Jenkins, A. Kirwan, P. J. Nolan, D. J. Thornley, S. M. Mullins, R. Wadsworth, and R. A. Wyss, J. Phys. G **15**, 671 (1989).

[14]E. S. Paul, D. B. Fossan, Y. Liang, R. Ma, and N. Xu, Phys. Rev. C **40**, 1255 (1989).

[15]E. S. Paul, D. B. Fossan, Y. Liang, R. Ma, N. Xu, R. Wadsworth, I. Jenkins, and P. J. Nolan, Phys. Rev. C **41**, 1576 (1990).

[16]R. Ma, E. S. Paul, C. W. Beausang, S. Shi, N. Xu, and D. B. Fossan, Phys. Rev. C **36**, 2322 (1987).

[17]W. F. Piel, Jr., C. W. Beausang, D. B. Fossan, L. Hildingsson, and E. S. Paul, Phys. Rev. C **35**, 959 (1987).

[18]R. Ma, C. W. Beausang, E. S. Paul, W. F. Piel, Jr., S. Shi, N. Xu, D. B. Fossan, J. Burde, M. A. Deleplanque, R. M. Diamond, A. O. Macchiavelli, and F. S. Stephens, Phys. Rev. C **40**, 156 (1989).

[19]R. Ma, K. Ahn, D. B. Fossan, Y. Liang, E. S. Paul, and N. Xu, Phys. Rev. C **39**, 530 (1989).

[20]Ch. Droste, W. Neubert, J. Lewitowicz, S. Chojnacki, T. Morek, Z. Wilhelmi, and K. F. Alexander, Nucl. Phys. **A152**, 579 (1970).

[21]J. Gizon, A. Gizon, M. R. Maier, R. M. Diamond, and F. S. Stephens, Nucl. Phys. **A222**, 557 (1974).

[22]A. Zemel, C. Broude, E. Dafni, A. Gelberg, M. B. Goldberg, J. Gerber, G. J. Kumbartzki, and K.-H. Speidel, Z. Phys. A **304**, 269 (1982).

[23]L. Hildingsson, C. W. Beausang, D. B. Fossan, W. F. Piel, Jr., A. P. Byrne, and G. D. Dracoulis, Nucl. Instrum. Methods **A252**, 91 (1986).

[24]G. Palameta and J. C. Waddington, Nucl. Instrum. Methods **A234**, 476 (1985).

[25]T. Yamazaki, Nucl. Data **A3**, 1 (1967).

[26]E. der Mateosian and A. W. Sunyar, At. Data Nucl. Data Tables **13**, 391 (1974).

[27]R. D. Gill, *Gamma-ray Angular Correlations* (Academic, New York, 1975), p. 180.

[28]K. S. Krane, R. M. Steff, and R. M. Wheeler, Nucl. Data Tables **A11**, 351 (1973).

[29]R. Bengtsson and S. Frauendorf, Nucl. Phys. **A327**, 139 (1979).

[30]S. M. Harris, Phys. Rev. **138**, B509 (1965).

[31]J. Gizon, A. Gizon, and D. J. Horen, Nucl. Phys. **A252**, 509 (1975).

[32]K. Ahn, Y. Liang, R. Ma, E. S. Paul, N. Xu, and D. B. Fossan (unpublished).

[33]R. Wyss, A. Johnson, J. Nyberg, R. Bengtsson, and W. Nazarewicz, Z. Phys. A **329**, 255 (1988).

[34]F. Dönau and S. Frauendorf, in *Proceedings of the Conference on High Angular Momentum Properties of Nuclei* (Ref. 7), p. 143; F. Dönau, Nucl. Phys. **A471**, 469 (1987).